AAPT PHYSICS EDUCATION | AMERICAN JOURNAL of PHYSICS

A simplified approach to synchrotron radiation

B. D. Patterson

Citation: American Journal of Physics **79**, 1046 (2011); doi: 10.1119/1.3614033
View online: http://dx.doi.org/10.1119/1.3614033
View Table of Contents: http://scitation.aip.org/content/aapt/journal/ajp/79/10?ver=pdfcov
Published by the American Association of Physics Teachers

A simplified approach to synchrotron radiation

B. D. Patterson
Paul Scherrer Institute, CH-5232 Villigen, Switzerland

(Received 7 May 2010; accepted 28 June 2011)

Synchrotron radiation is examined in a simple and pedagogical way. The approach is that of Feynman and provides an intuitive, but rigorous graphical interpretation of the distinction between true and apparent relativistic electron motion. Feynman's demonstration that the apparent motion in the field of a bending magnet follows a curtate cycloid is augmented by a novel derivation of the emission spectrum. A similar graphical analysis is applied to insertion device radiation, to highlight the distinction between a wiggler and an undulator. © *2011 American Association of Physics Teachers.*
[DOI: 10.1119/1.3614033]

I. INTRODUCTION

Synchrotron radiation is emitted by relativistic electrons, whose trajectories are bent by the Lorentz force of an applied magnetic field $\boldsymbol{B}$. Motion in a uniform magnetic field results in *bending-magnet radiation*. Periodic magnetic arrays, known as *insertion devices*, can be used to increase the spectral flux; prime examples are high-deflection *wigglers* and low-deflection *undulators*. The bending-magnet radiation spectrum is a broad continuum around the characteristic or *critical* frequency $\omega_c = 3\gamma^2 eB/2m$. Here $-e$ and m are the electron charge and mass, respectively, the relativistic factor is $\gamma = \left(1-\beta^2\right)^{-1/2} = E_{\mathrm{el}}/(mc^2)$, $\beta = v/c$ is the ratio of the electron speed to the speed of light, and E_{el} is the electron energy. For an electron energy of several GeV ($\gamma \sim 5000$) and a magnetic field of approximately 1 T, ω_c corresponds to an X-ray frequency.

Synchrotron radiation originates in a small area (the cross section of the electron beam is typically tens of micrometer) and is highly collimated, with a divergence angle of approximately $1/\gamma \sim 0.01°$. The relativistic electron motion leads to a γ^2 increase in the spectral flux density. Spectral filtering of the broadband bending-magnet radiation or altering the undulator field strength allows the wavelength to be tuned, and the circulating electron packets in the synchrotron generate short-duration (~100 ps) pulses suitable for time-resolved experiments.

The radiation is generally linearly polarized, but circular polarization can be obtained above or below the orbit plane of a bending magnet and from the special helical undulators. Synchrotron radiation beams have become the tool of choice for challenging experiments involving X-ray diffraction, and imaging and spectroscopy in chemistry,[1] structural biology,[2] condensed matter physics,[3,4] and materials science.[5]

The use of synchrotron radiation is rapidly developing. This growth implies that the nonexperts are often confronted with the problem of finding a correct but understandable explanation of the underlying principles of the generation of synchrotron radiation. Standard textbook treatments of synchrotron radiation[6–10] are based on an analytic Lorentz transformation from the electron to the laboratory frame and require the complex evaluation of retarded expressions.

In this paper, we provide a graphical but rigorous approach. We begin with a repetition of the elegant treatment of radiation by a relativistic electron due to Feynman,[11,12] which in effect graphically performs the Lorentz transformation, and we then extend it to calculate the emission spectrum of synchrotron radiation from a bending magnet. The same graphical approach is used to treat insertion-device radiation and to distinguish between a wiggler and an undulator.

Synchrotron radiation was discovered[13] at the GE Research Laboratory in 1947, and several excellent textbooks on its applications are available.[14–18] A simulation[19] of the generation of synchrotron radiation illustrates several of the concepts treated in the present work. The highly informative *X-ray Data Booklet*[20] lists 46 synchrotron radiation facilities worldwide. An entertaining approach to the subject of synchrotron radiation and its applications is offered by the textbook and online lectures of Attwood.[21]

II. RADIATION BY A MOVING ELECTRON

The discussion in this section is from Feynman *et al.*[11,12] We consider an electron moving along the path $\vec{r}(\tau)$, as seen by an observer at the point (x,y,z). We distinguish between τ, the time in the frame of the electron (the *emitter time*) and t, the time in the observer's frame (the *observer time*); $\vec{r}(\tau)$ is the *true* path of the electron, and $\vec{r}'(t)$ is the *apparent* path of the electron. Feynman gives a rigorous expression for the electric and magnetic fields of the moving electron, an expression which is also derived by Kim[6]

$$\vec{E}(x,y,z) = \frac{e}{4\pi\varepsilon_0}\left[\frac{\hat{r}'}{r'^2} + \frac{r'}{c}\frac{d}{dt}\left(\frac{\hat{r}'}{r'^2}\right) + \frac{1}{c^2}\frac{d^2\hat{r}'}{dt^2}\right], \tag{1a}$$

$$\vec{B} = \frac{-1}{c}\hat{r}' \times \vec{E}. \tag{1b}$$

The first term in $\vec{E}(x,y,z)$, the near-field term, is the familiar $1/r^2$ Coulomb law, and the second term is a relativistic correction. Of interest here is the third, radiation term, $\vec{E}_{\mathrm{rad}}$, which in the far-field limit decreases more slowly as $1/r$. Complications arise in Eq. (1) from the appearance of the apparent position $\vec{r}'$ and the observer time t, which, for relativistic motion, may differ dramatically from the true position $\vec{r}$ and the emitter time τ. For example, suppose that we observe from the position $z = R_0$ the motion of an electron following the true trajectory $\vec{r}(\tau)$ in the vicinity of the origin. In Fig. 1, the positions of the observer and electron are indicated (in two dimensions), along with the apparent position of the electron $\vec{r}' = (x',z')$ and the corresponding unit vector $\hat{r}'$. Note that $\hat{r}'$ points from the observer toward the electron. For a distant observer ($x' \ll R_0$, $z' \approx -R_0$) we have

$$\hat{r}' = \frac{x'\hat{x} + z'\hat{z}}{\sqrt{x'^2 + z'^2}} \approx \left(\frac{x'}{R_0}\right)\hat{x} - \hat{z}, \tag{2}$$

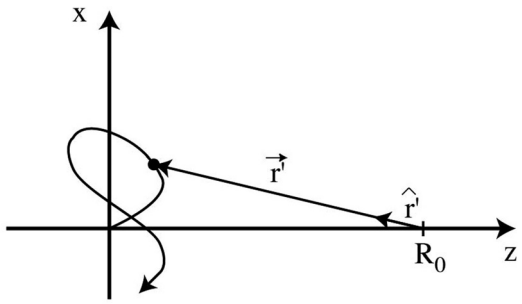

Fig. 1. The motion of an electron near the origin is followed by an observer at $z = R_0$.

and the radiation term in the expression for $\vec{E}$ becomes

$$\vec{E}_{\text{rad}} = \frac{e}{4\pi\varepsilon_0 c^2}\frac{d^2\hat{r}'}{dt^2} \approx \frac{e}{4\pi\varepsilon_0 c^2}\frac{d^2}{dt^2}\left(\frac{x'}{R_0}\right)\hat{x}, \tag{3a}$$

$$\approx \frac{e}{4\pi\varepsilon_0 c^2 R_0} a'_{\perp}(t)\hat{r}_{\perp}. \tag{3b}$$

Note that the radiation field decreases with distance as $1/R_0$, is perpendicular to the electron-observer direction and is proportional to the transverse component of the apparent acceleration.

III. TRUE AND APPARENT ELECTRON MOTION IN A BENDING MAGNET

From a distant vantage point at $z = R_0$, we now consider the motion of an electron that follows the circular trajectory shown in Fig. 2(a). A segment of this trajectory near time zero will correspond to that in a bending magnet. Because of the nonzero propagation time of light over the distance $R_0 - z$, the observer time t associated with the emitter time τ for an electron with coordinate $z(\tau)$ is given by

$$t = \tau + \frac{R_0}{c} - \frac{z(\tau)}{c}. \tag{4}$$

In what follows, we disregard the constant term R_0/c.

As shown in Fig. 2(a), the true path $\vec{r}(\tau)$ of the electron is the dark electron circle. A point moving with the same angular velocity on the slightly larger circle moves with speed c. In Fig. 2(b), we use a graphical method to construct from the true x-coordinate $x(\tau)$ (points) the apparent position $x'(t)$

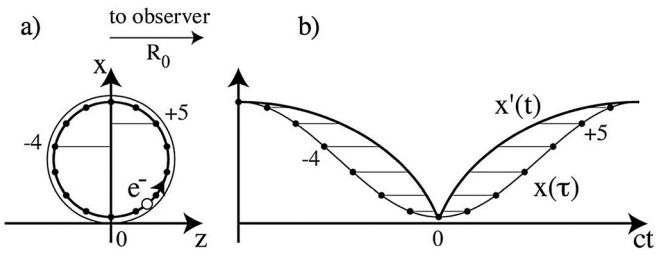

Fig. 2. (a) An electron undergoes circular motion at an orbital electron radius r. (b) Its apparent x-position $x'(t)$ is obtained from the true position $x(\tau)$ by a translation along the time-axis by the light propagation time z/c. This procedure yields a curtate cycloid for $x'(t)$, which is equivalent to the path traced out by the position of the electron at $t = 0$ as the diagram in (a) is unrolled along the circle with larger (light) radius $R = r/\beta$. This figure is adapted from Ref. 12.

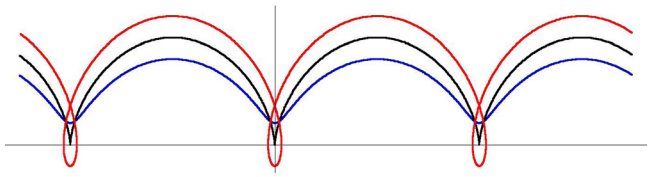

Fig. 3. The cycloid family, comprising the curtate cycloid (lower curve, corresponding to particle motion with $v < c$; electron radius < light radius), the cycloid (middle curve; $v = c$; electron radius = light radius) and the prolate cycloid (upper curve; $v > c$; electron radius > light radius). For $v = c$, the cusps are infinitely sharp.

(dark curve). Each of the $x(\tau)$ points is shifted in time to account for the light propagation. Consider, for example, point -4. Because it is more distant from the observer than the origin, the apparent time is later than the true time, and we move the point in Fig. 2(b) to the right by the corresponding line segment in Fig. 2(a). Analogously, point $+5$ undergoes a shift to earlier time. The result for the apparent particle trajectory $x'(t)$ is a curtate cycloid (incorrectly called a hypocycloid by Feynman), which belongs to the family of cycloids shown in Fig. 3. Of particular importance for synchrotron radiation is the sharp cusp in $x'(t)$, which occurs at the moment when the electron moves directly toward the observer ($t = 0$). At this point in the trajectory, the large apparent transverse acceleration causes the emission of an intense burst of synchrotron radiation.

IV. CYCLOID CONSTRUCTION

As stated, the electron moves with speed $v = \beta c$ on the electron circle of radius r, with the orbital frequency ω_0 equal to the phase angle φ divided by the emitter time τ, while a corresponding point on the slightly larger circle of radius $R = r/\beta$ moves at the speed c, so that

$$\omega_0 \equiv \frac{\varphi}{\tau} = \frac{c}{R} = \frac{c\beta}{r} \tag{5}$$

Note that for an electron moving at exactly speed c, the two circles coincide. For a 2.4 GeV electron typical of a medium energy synchrotron, $\gamma \approx 4700$, and hence the difference between R and r is very small and is given by

$$R - r = R(1-\beta) \approx \frac{R}{2\gamma^2} = \frac{c}{2\omega_0\gamma^2} \qquad (\gamma \gg 1). \tag{6}$$

From the construction in Fig. 4, we see that

$$c\tau = \varphi R, \tag{7a}$$

$$ct = c\tau - r\sin\varphi, \tag{7b}$$

$$x' = R - r\cos\varphi. \tag{7c}$$

The generation of the apparent path $x'(t)$ proceeds as follows. We choose a value for t, and from the relation $ct = R\varphi - r\sin\varphi$, we numerically obtain the corresponding value of $\varphi(t)$. We then calculate $x'(t) = R - r\cos[\varphi(t)]$. The results are shown in Fig. 5.

V. SERIES APPROXIMATION

It is not possible to obtain an exact analytical description of the curtate cycloid. Because we are principally interested

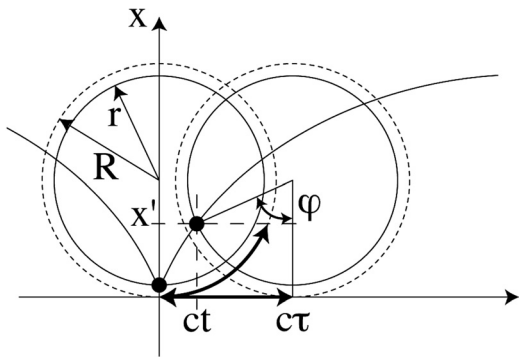

Fig. 4. Construction of the apparent curtate cycloidal path (solid curve) of a particle moving on the electron circle r by unrolling along the (dotted) light circle R.

in the region of high apparent acceleration corresponding to motion toward the observer, we define this instant as time zero (for both the emitter and the observer), and we perform a series approximation to $x'(t)$ by assuming a third-order polynomial expansion for $\varphi(t)$ near $t=0$,

$$\phi(t) \approx a_1(ct) + a_2(ct)^2 + a_3(ct)^3. \tag{8}$$

From Eq. (7), we obtain the relation $\varphi R - r\sin\varphi = ct$ and by expanding the sine function and equating orders, we obtain the following values for the coefficients a_i:

$$a_1 = \frac{1}{R-r}, \tag{9a}$$

$$a_2 = 0, \tag{9b}$$

$$a_3 = \frac{-r}{6(R-r)^4}. \tag{9c}$$

Thus we can write

$$\varphi \approx \frac{ct}{R-r}\left(1 - \frac{rc^2t^2}{6(R-r)^3}\right) \approx 2\omega_0\gamma^2 t\left(1 - \frac{4}{3}\omega_0^2\gamma^6 t^2\right) = \omega_0\tau. \tag{10}$$

Sufficiently close to $t=0$, we can ignore the t^2 term in the parenthesis of Eq. (10), yielding $t \approx \tau/2\gamma^2$. If we use the relativistic approximation $\beta = \sqrt{1-\gamma^{-2}} \approx 1 - 1/2\gamma^2$, we see that this result for t is in agreement with the on-axis time squeezing factor of Kim,[6] $t = \tau(1-\beta)$. The true electron trajectory has effectively been squeezed into the sharp cusp of the apparent trajectory due to the finite speed of light.

We can now use the series expansion (10) for φ to obtain a polynomial expansion for the apparent path $x'(t)$ near the cusp

$$x'(t) = R - r\cos\varphi = \frac{c}{\omega}(1 - \beta\cos\varphi), \tag{11a}$$

$$\approx \frac{c}{2\omega_0\gamma^2} + 2\omega_0 c\gamma^4 t^2 - \frac{16}{3}\omega_0^3 c\gamma^{10} t^4, \tag{11b}$$

and hence for the apparent (transverse) acceleration we have

$$a'_\perp(t) = \frac{d^2x'(t)}{dt^2} \approx 4\omega_0 c\gamma^4\left(1 - 16\omega_0^2 t^2\gamma^6\right). \tag{12}$$

Note that Eq. (12) for $a'_\perp(t)$ has zeros at $t \equiv \pm\Delta t/2 = \pm 1/(4\omega_0\gamma^3)$, which span the region of high apparent acceleration.

We compare the polynomial expression with the numerical calculation in Fig. 6. Note the following features of $a'_\perp(t)$: The peak apparent acceleration is proportional to γ^4, the apparent duration of the high acceleration is approximately $\Delta t = 1/(2\omega_0\gamma^3)$, and the true duration is $\Delta\tau = 2\gamma^2\Delta t = 1/(\omega_0\gamma)$. Thus, the opening angle of the radiation is $\Delta\varphi = \omega_0\Delta\tau = 1/\gamma$, and hence the circulating charge radiates tangentially a searchlight beam with divergence $1/\gamma$ (see Fig. 7).

From the equivalence of the centripetal rate of change of momentum and the Lorentz force, we obtain $\gamma m\dot{v} = evB \approx ecB$, and from the definitions of centripetal acceleration and angular velocity, we have $\dot{v} = \omega_0^2 r$ and $\omega_0 \approx c/r$, yielding $r = \gamma mc/eB$ and $\omega_0 = eB/\gamma m$.

VI. TYPICAL PHOTON ENERGY

From Fig. 7, we conclude that a tangentially-situated observer sees an intense burst of synchrotron radiation when the emitting electron is moving directly toward him/her. From Fourier synthesis arguments, this short burst, with the apparent duration $\Delta t \sim 1/(\gamma^3\omega_0)$, will contain typical frequency components of order $\omega \sim 1/\Delta t \sim \gamma^2 eB/m$. The characteristic energy for synchrotron-radiation photons is defined as[6]

$$\hbar\omega_c \equiv \frac{3}{2}\frac{\gamma^2\hbar eB}{m} = 0.665E_{el}^2[\mathrm{GeV}]B[\mathrm{T}]\mathrm{keV}. \tag{13}$$

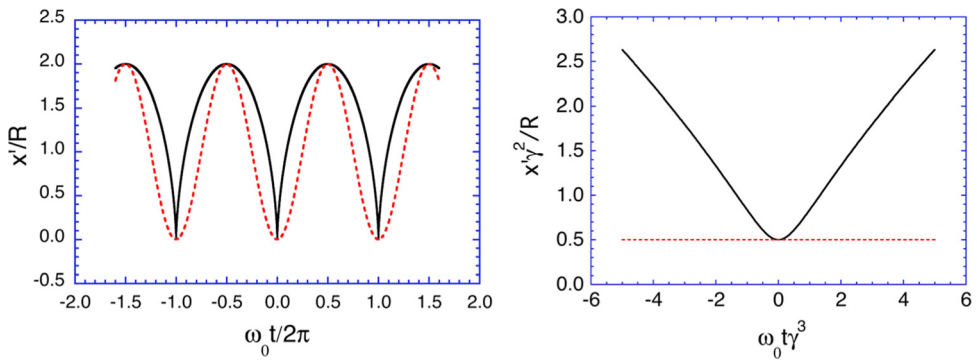

Fig. 5. The computed apparent curtate cycloidal path $x'(t)$ (solid curves) compared to the true path $x(\tau)$ (dotted curves). Note that the horizontal and the vertical scales in the right-hand plot have been scaled by γ^3 and γ^2, respectively, to make the cusp at $t=0$ visible. This scaling makes the $x'(t)$ curve near $t=0$ independent of the value of γ (for $\gamma \gg 1$).

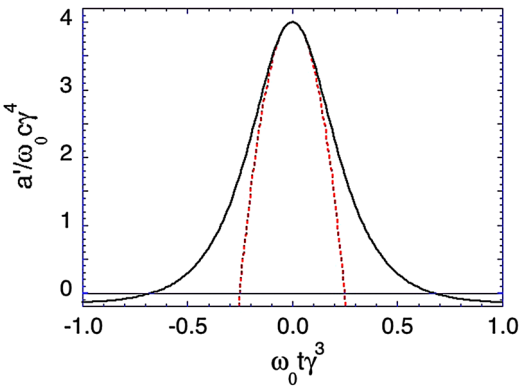

Fig. 6. A scaled comparison of the second-order polynomial (dotted curve) and numerical expression (solid curve) for the apparent acceleration near the cusp at $t=0$.

For an electron energy of 2.4 GeV ($\gamma = E_{\rm el}$[GeV]/0.000511) and a bending magnet field of 1.6 T, Eq. (13) implies that $\hbar\omega_c = 6.1$ keV, corresponding to a photon in the hard X-ray regime. In the absence of relativistic effects, the electron would emit dipole radiation at the orbital frequency $\omega_0/2\pi = 9.5$ MHz.

VII. SPECTRAL FLUX DENSITY

We now extend Feynman's graphical construction to a calculation of the spectrum of the bending-magnet radiation, beginning with Eq. (3) for the radiation field $E_x(t) = E_{\rm rad}$ and its Fourier transform $E_x(\omega)$

$$E_x(t) = \frac{e}{4\pi\varepsilon_0 c^2 R_0} a'_\perp(t) \equiv \frac{1}{\sqrt{2\pi}}\int_{-\infty}^{\infty} E_x(\omega) e^{-i\omega t} d\omega, \tag{14a}$$

$$E_x(\omega) = \frac{1}{\sqrt{2\pi}}\int_{-\infty}^{\infty} E_x(t) e^{i\omega t} dt = \frac{e}{32^{1/2}\pi^{3/2}\varepsilon_0 c^2 R_0}\int_{-\infty}^{\infty} a'_\perp(t) e^{i\omega t} dt. \tag{14b}$$

The energy density (energy per solid angle $d\Omega^2$) emitted by a single electron is given by the time integral of the Poynting vector $\vec{S} = \varepsilon_0 c^2 \vec{E} \times \vec{B}$

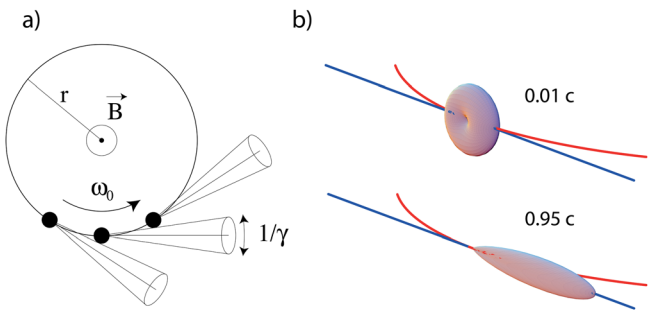

Fig. 7. (a) A schematic of the rotating searchlight synchrotron beam with opening angle $1/\gamma$. (b) Computed dipole emission patterns (from expressions in Ref. 7) for electron velocities $v = 0.01\ c$ and $0.95\ c$.

$$\frac{d^2W}{d\Omega^2} = R_0^2\frac{d^2W}{dxdy} = R_0^2\int |\vec{S}(t)|dt = R_0^2\varepsilon_0 c^2\int E_x(t)B_y(t)dt = R_0^2\varepsilon_0 c\int |E_x(t)|^2 dt. \tag{15}$$

If we consider only a single pulse of radiation, we can extend the limits of integration to $\pm\infty$

$$\frac{d^2W}{d\Omega^2} = R_o^2\varepsilon_0 c\int_{-\infty}^{\infty}|E_x(t)|^2dt = R_0^2\varepsilon_0 c\int_{-\infty}^{\infty}|E_x(\omega)|^2 d\omega = 2R_0^2\varepsilon_0 c\int_0^{\infty}|E_x(\omega)|^2 d\omega, \tag{16}$$

where we used the fact that $\frac{1}{2\pi}\int_{-\infty}^{\infty} e^{i(\omega-\omega')t}dt = \delta(\omega-\omega')$. We thus find that the spectral energy density radiated by a single electron is given by

$$\frac{d^3W}{d\Omega^2 d\omega} = 2R_o^2\varepsilon_0 c|E(\omega)|^2 = \frac{e^2}{16\pi^3\varepsilon_0 c^3}\left|\int_{-\infty}^{\infty} a'_\perp(t)e^{i\omega t}dt\right|^2 \tag{17}$$

By (incoherently) adding the effects of $I_{\rm el}/e$ electrons per second, where $I_{\rm el}$ is the electron current in the synchrotron, and dividing by the photon energy, we obtain the spectral photon flux density

$$\frac{d^2F}{d\Omega^2} = \frac{1}{\hbar\omega}\frac{I_{el}}{e}\frac{d^3W}{d\Omega^2 d\omega}\Delta\omega. \tag{18}$$

VIII. PARAMETRIC INTEGRATION

To evaluate the integral in Eq. (17) for the spectral energy density, we perform a change of variable from the apparent time t to the rotation phase angle φ, which is proportional to the emitter time τ. From the construction of the curtate cycloid, we have

$$\begin{pmatrix} x'(\varphi) \\ ct(\varphi)\end{pmatrix} = \begin{pmatrix} R - r\cos\varphi \\ R\varphi - r\sin\varphi\end{pmatrix}. \tag{19}$$

We therefore obtain

$$\frac{dt(\varphi)}{d\varphi} = \frac{1}{c}(R - r\cos\varphi). \tag{20}$$

In terms of φ, the x-component of the apparent velocity becomes

$$v'_\perp(\varphi) = \frac{dx'}{dt} = \frac{dx'(\varphi)}{d\varphi}\left[\frac{dt(\varphi)}{d\varphi}\right]^{-1} = \frac{rc\sin\varphi}{R - r\cos\varphi}, \tag{21}$$

and the x-component of the apparent acceleration is

$$a'_\perp(\varphi) = \frac{dv'_\perp}{dt} = \frac{dv'_\perp(\varphi)}{d\varphi}\left[\frac{dt(\varphi)}{d\varphi}\right]^{-1} = \frac{-rc^2(r - R\cos\varphi)}{(R - r\cos\varphi)^3}. \tag{22}$$

We can then express the time integral in Eq. (17) as

$$\int a'_\perp(t)e^{i\omega t}dt = \int a'_\perp(t)e^{i\omega t}\frac{dt(\varphi)}{d\varphi}d\varphi$$
$$= \int \frac{-rc(r - R\cos\varphi)}{(R - r\cos\varphi)^2} e^{i\omega(R\varphi - r\sin\varphi)/c} d\varphi \quad (23)$$

Note that $r = \beta R \approx R(1 - (1/2\gamma^2))$, the important interval for φ is of order $1/\gamma$, and hence we can use the small-angle approximations $\cos\varphi \approx 1 - \varphi^2/2$ and $\sin\varphi \approx \varphi - \varphi^3/6$. If we define the variable $u = \gamma\varphi$, and we recall the critical photon frequency in Eq. (13), $\omega_c = 3\gamma^2 eB/2m = 3\gamma^3 c/2r \approx 3\gamma^3 c/2R$, we find

$$\int_{-\infty}^{\infty} a'_\perp(t)e^{i\omega t}dt \approx 2\gamma c \int_{-\infty}^{\infty} \frac{1-u^2}{(1+u^2)^2} \times \exp\left[i\frac{3\omega}{4\omega_c}\left(u + \frac{u^3}{3}\right)\right] du$$
$$= 4\gamma c \int_0^{\infty} \frac{1-u^2}{(1+u^2)^2} \cos\left[\frac{3\eta}{2}\left(u + \frac{u^3}{3}\right)\right] du, \quad (24)$$

where $\eta \equiv \frac{\omega}{2\omega_c}$. We define $U = \cos\left[\frac{3\eta}{2}\left(u + \frac{u^3}{3}\right)\right]$ and $dV = \frac{1-u^2}{(1+u^2)^2}du$, and perform the integration in Eq. (24) by parts to obtain

$$\int UdV = UV - \int VdU$$
$$= \left\{\cos\left[\frac{3\eta}{2}\left(u + \frac{u^3}{3}\right)\right]\left(\frac{u}{1+u^2}\right)\right\}\Bigg|_0^{\infty}$$
$$- \int_0^{\infty}\left(\frac{u}{1+u^2}\right)\left\{-\frac{3\eta(1+u^2)}{2} \times \sin\left[\frac{3\eta}{2}\left(u + \frac{u^3}{3}\right)\right]\right\} du \quad (25a)$$
$$= 0 + \frac{\sqrt{3}}{4}\frac{\omega}{\omega_c}K_{2/3}\left(\frac{\omega}{2\omega_c}\right) \quad (25b)$$

We have introduced the modified Bessel function[22]

$$K_{2/3}(\eta) = \sqrt{3}\int_0^{\infty} u\sin\left[\frac{3}{2}\eta\left(u + \frac{u^3}{3}\right)\right] du. \quad (26)$$

We thus reproduce the conventional formula for the spectral flux density given by Kim[6]

$$\frac{d^2F}{d\Omega^2} = \frac{\alpha}{\pi^2}\gamma^2\frac{I_{el}}{e}\frac{\Delta\omega}{\omega}\left[\frac{3}{4}\left(\frac{\omega}{\omega_c}\right)^2 K^2_{2/3}\left(\frac{\omega}{2\omega_c}\right)\right], \quad (27)$$

where $\alpha = e^2/4\pi\varepsilon_0\hbar c$ is the fine-structure constant. In terms of practical units, Eq. (27) becomes

$$\frac{d^2F}{d\Omega^2}\left[\text{ph/s/mrad}^2/0.1\%\text{bw}\right]$$
$$= 1.33\times 10^{33} E^2_{el}[\text{GeV}] I_{el}[\text{A}]\left(\frac{\omega}{\omega_c}\right)^2 K^2_{2/3}\left(\frac{\omega}{2\omega_c}\right), \quad (28)$$

giving the spectral flux per mrad^2 solid angle and per 0.1% photon energy bandwidth.

If we use the approximate expression for $K_{2/3}$ given in Ref. 23, and use the values for a bending magnet at the Swiss Light Source ($E_{el} = 2.4$ GeV, $I_{el} = 0.4$ A, $B = 1.6$ T), we can plot $d^2F/d\Omega^2$ as a function of photon energy as in Fig. 8.

IX. INSERTION DEVICES

An insertion device (ID), that is, a wiggler or an undulator, presents relativistic electrons with a large number of alternately-poled magnets, in a periodic structure with period λ_u (see Fig. 9). A pedagogical discussion of undulator radiation is found in Ref. 24. We assume a simple cosine dependence of the magnetic field, $B_y = B_0\cos(k_u z)$, where $k_u \equiv 2\pi/\lambda_u$. The Lorentz force exerted by the insertion device magnets on the electrons yields the equations of motion

$$\gamma m\ddot{z} = -e\dot{x}B_y, \quad (29a)$$
$$\gamma m\ddot{x} = e\dot{z}B_y. \quad (29b)$$

For large γ we can solve for the electron trajectory by initially assuming that $\dot{z} \approx$ constant $\equiv \bar{\beta}c \gg \dot{x}$. The solution for the x-component of the velocity is given by

$$\dot{x} = \frac{cK}{\gamma}\sin\omega_u\tau, \quad (30)$$

where $\omega_u \equiv k_u\bar{\beta}c$ and $K = eB_0\lambda_u/2\pi mc$ is the dimensionless *undulator parameter*. From the relation $\dot{x}^2 + \dot{z}^2 = \beta^2c^2$, we obtain, to order $1/\gamma^2$,

$$\dot{z} = \left[1 - \frac{1}{2\gamma^2}\left(1 + K^2\cos^2\omega_u\tau\right)\right]c \quad (31a)$$
$$\langle\dot{z}\rangle = \bar{\beta}c = \left[1 - \frac{1}{2\gamma^2}\left(1 + \frac{K^2}{2}\right)\right]c, \quad (31b)$$

where the average in Eq. (31b) is taken over many periods. We integrate over τ and obtain the true electron trajectory

$$x(\tau) = \frac{-cK}{\gamma\omega_u}\cos\omega_u\tau \quad (32a)$$
$$z(\tau) = \bar{\beta}c\tau + \frac{cK^2}{8\gamma^2\omega_u}\sin 2\omega_u\tau \quad (32b)$$

which is plotted in Fig. 10.

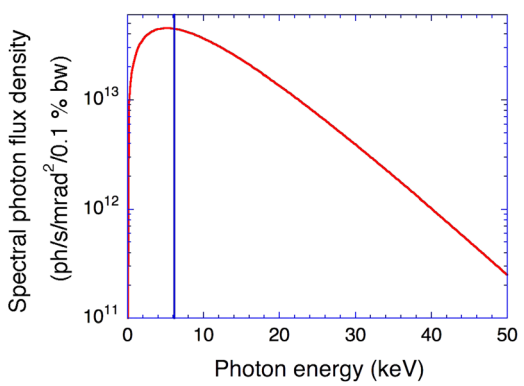

Fig. 8. The spectral photon flux density from Eq. (28) for a bending magnet at the Swiss Light Source. The critical photon energy $\hbar\omega_c = 6.1$ keV (vertical line) divides the spectrum into halves with equal emitted power.

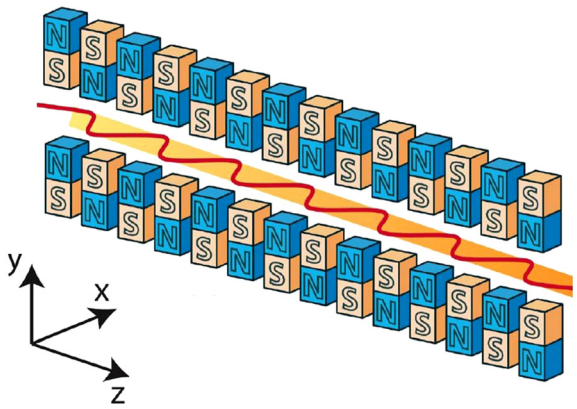

Fig. 9. Electron motion along an insertion device: a wiggler or an undulator.

The maximum deflection angle of the electron by the insertion device field is

$$\delta = \arctan\left(\frac{\dot{x}}{\dot{z}}\right)\Big|_{\omega_u\tau=\pi/2} \approx \frac{K}{\gamma}, \tag{33}$$

which is K times the opening angle $1/\gamma$ for the emission of synchrotron radiation. If $K \gg 1$, the individual poles radiate independently from one another, such as a collection of bending magnets, and we refer to the insertion device as a *wiggler*. For K smaller than or of the order of unity, we speak of an *undulator*.

To find the apparent electron trajectory through the insertion device, we again assume that the observer is at the large positive distance $z = R_0$, and account for the finite time of light propagation according to $t = \tau + (R_0/c) - z(\tau)/c$. As for the bending magnet, we obtain the apparent motion $x'(t)$ by shifting the time coordinate of the true motion $x(\tau)$ by the intervals given by the fine lines in Fig. 10.

From the construction in Fig. 11 we see that $\lambda = \lambda_u/\bar{\beta} - \lambda_u$, from which, using Eq. (31), we derive the *undulator equation* for the on-axis, fundamental radiated wavelength

$$\lambda \approx \frac{\lambda_u}{2\gamma^2}\left(1 + \frac{K^2}{2}\right) \tag{34}$$

Note how, for the large K-value of Figs. 10 and 11 (wiggler case), sharp cusps again appear in the apparent trajectory when the electron is moving toward the observer. As for the bending magnet, these will be responsible for the emission

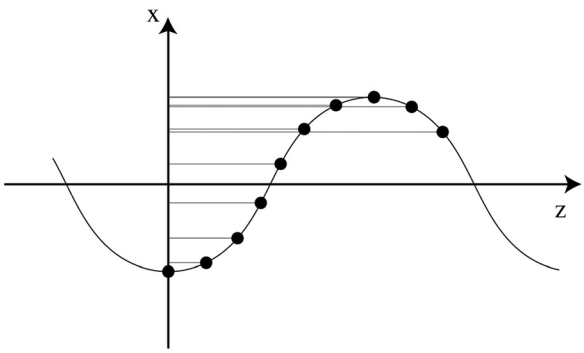

Fig. 10. The true electron trajectory in an insertion device with $K = 10$. Note the departure from a cosine curve.

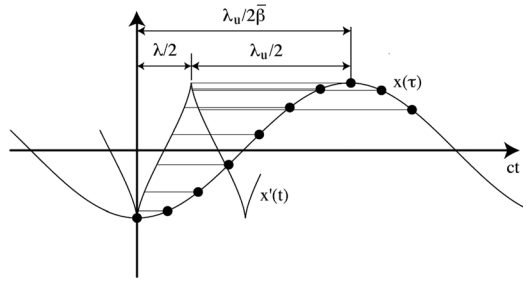

Fig. 11. Graphical construction from the true electron trajectory $x(\tau)$ of the apparent trajectory $x'(t)$ for a wiggler with $K = 10$.

of intense, broadband synchrotron radiation. The apparent $x'(t)$ trajectories and the associated apparent accelerations $a'_x(t)$ for the wiggler and undulator cases, $K = 3$ and $K = 0.6$, respectively, are compared in Fig. 12.

We can now use Eqs. (17) and (18) to compute the spectral photon flux density for the insertion device by numerically performing a Fourier transform of the apparent acceleration. The result is shown in Fig. 13. Note that the resulting wiggler spectrum (many thin vertical lines) is a semi-continuum, while the undulator spectrum (few thicker vertical lines) consists of a series of well-separated (odd) harmonics of the fundamental photon energy given by the undulator equation. From Eq. (34), we see that by varying K, for example, via the undulator field, we may tune the fundamental wavelength.

We define N_{per} as the number of magnetic periods of the wiggler, implying that the wiggler emission is the sum of the radiation fields from the $2N_{\text{per}}$ separate wiggler poles. Because each period of the apparent acceleration (see Fig. 12) is anti-symmetric with respect to the zero-crossing time point, the fast Fourier transform algorithm applied over N_{per} wiggler periods results in a series of sharp peaks at the odd harmonics of the fundamental frequency, and the frequency interval between each pair of neighboring peaks is sampled at $2N_{\text{per}}$ frequency points. Smoothing the wiggler spectrum to account for the limited beamline resolution is thus equivalent to dividing the peak values by $2N_{\text{per}}$, which yields the dashed curve in Fig. 13.

The radiation from a wiggler is effectively equivalent to that from $2N_{\text{per}}$ bending magnets, each of which has the magnetic field $B = B_0 = 2\pi mcK/e\lambda_u$, and hence, the characteristic synchrotron radiation frequency $\omega_c = 3\pi K\gamma^2 c/\lambda_u$. We may verify numerically that the resolution-averaged spectral photon flux density for the $K = 3$ wiggler (dashed curve in Fig. 13) is identical to the corresponding bending magnet

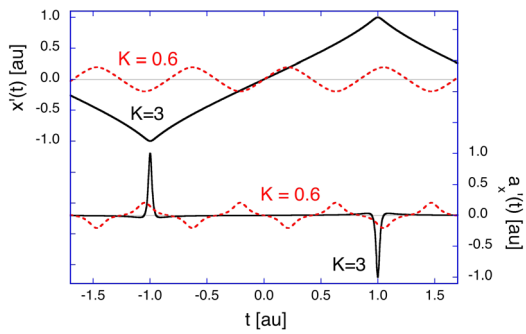

Fig. 12. Apparent trajectories $x'(t)$ and the associated apparent accelerations $a_x'(t)$ for an undulator ($K = 0.6$, dotted curves) and a wiggler ($K = 3$, solid curves).

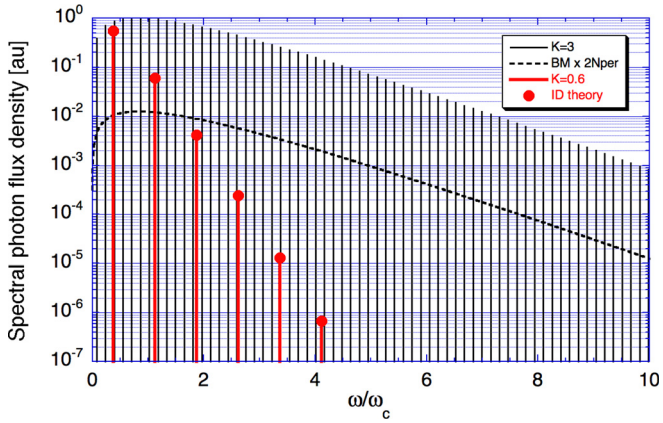

Fig. 13. The spectral photon flux density (in arbitrary, but consistent, units and on a logarithmic scale) for insertion devices with $K=0.6$ (undulator, few thick vertical lines) and $K=3$ (wiggler, many thin vertical lines), calculated by computing the Fourier transform of the apparent acceleration from Fig. 12. The number of insertion device periods in each case is $N_{\text{per}}=41$. The filled circles are from the expression for an undulator in Eq. (35) with $K=0.6$, and the dashed curve is the frequency-averaged wiggler spectrum, equal to $2N_{\text{per}}$ times the $K=3$ bending magnet spectrum. The abscissa gives the radiation frequency in units of the $K=3$ critical frequency ω_c.

spectrum from Eq. (27), increased by the factor $2N_{\text{per}}$. We thus conclude that the peak spectral flux density emitted by an insertion device exceeds that of a single equivalent bending magnet by two factors of $2N_{\text{per}}$, that is, by $(2N_{\text{per}})^2$. One of these factors arises from the number of radiating poles. The second factor of $2N_{\text{per}}$ is a result of a narrowing of the emission solid angle. A treatment of off-axis emission from an insertion device is beyond our present discussion.

In the theoretical treatment of Kim,[6] it is shown that an insertion device emits on-axis only at odd harmonic numbers, n = 1,3,5,…, with a spectral photon flux density given by

$$\frac{d^2F^n}{d\Omega^2}=\alpha N_{per}^2\gamma^2\frac{I_{el}}{e}\frac{\Delta\omega}{\omega}\frac{K^2n^2}{(1+K^2/2)^2}\times\left\{J_{(n-1)/2}\left[\frac{nK^2}{4(1+K^2/2)}\right]-J_{(n+1)/2}\left[\frac{nK^2}{4(1+K^2/2)}\right]\right\}^2 \tag{35}$$

The points in Fig. 13 are calculated from Eq. (35) for $K=0.6$, demonstrating agreement with our (numerical) treatment of the undulator case.

X. SUMMARY

The exact graphical model of synchrotron radiation from Feynman's lectures on physics was presented in detail. Following Feynman, it is the apparent motion of the relativistic electron for a bending magnet along a curtate cycloid that determines the nature of the radiation field. Qualitative features of the radiation were discussed, including the emission pattern and the typical photon energy. Using Feynman's expression for the radiation field of an accelerated charge, the Poynting vector, and parametric integration, an expression was found for the radiation spectrum, which is identical to that from conventional treatments of synchrotron radiation. Feynman's graphical approach was applied to the case of insertion devices, highlighting the spectral differences between wiggler and undulator radiation.

ACKNOWLEDGMENTS

The author wishes to thank his colleagues B. Pedrini and M. Shalaby for their comments and assistance with the mathematical derivations.

[1]*Chemical Applications of Synchrotron Radiation*, edited by T.-K. Sham (World Scientific, Singapore 2002).
[2]J. R. Helliwell, *Macromolecular Crystallography with Synchrotron Radiation* (Cambridge U.P., Cambridge, 2005).
[3]*Magnetism and Synchrotron Radiation*, edited by E. Beaurepaire, H. Bulou, F. Scheurer, and J.-P. Kappler (Springer, Berlin, 2010).
[4]S. Ishihara and S. Maekawa, "Resonant X-ray scattering in manganites: Study of the orbital degree of freedom," Rep. Prog. Phys. **65**, 561–598 (2002).
[5]W. Reimers, A. R. Pyzalla, A. K. Schreyer, and H. Clemens, *Neutrons and Synchrotron Radiation in Engineering Materials Science* (John Wiley & Sons, New York, 2008).
[6]K.-J. Kim, "Characteristics of synchrotron radiation," AIP Conf. Proc. **184**, 565–632 (1989).
[7]J. D. Jackson, *Classical Electrodynamics*, 3rd ed. (John Wiley & Sons, New York, 1999).
[8]A. Hofmann, *The Physics of Synchrotron Radiation* (Cambridge U.P., Cambridge, 2004).
[9]P. Duke, *Synchrotron Radiation: Production and Properties* (Oxford U.P., Oxford, 2009).
[10]H. Wiedemann, *Synchrotron Radiation* (Springer, Berlin, 2010).
[11]R. P. Feynman, R. B. Leighton, and M. Sands, *The Feynman Lectures on Physics* (Addison-Wesley, New York, 1963), Vol. 1, Chap. 28.
[12]*ibid*, Chap. 34.
[13]H. C. Pollock, "The discovery of synchrotron radiation," Am. J. Phys. **51**, 278–280 (1983).
[14]G. Margaritondo and W. Weaver, *Synchrotron Radiation* (Am. Assoc. Phys. Teachers, New York, 1986).
[15]G. Margaritondo, *Introduction to Synchrotron Radiation* (Oxford U.P., Oxford, 1988).
[16]J. Als-Nielsen and D. McMorrow, *Elements of Modern X-Ray Physics* (John Wiley & Sons, New York, 2001).
[17]G. Margaritondo, *Elements of Synchrotron Light: For Biology, Chemistry and Medical Research* (Oxford U.P., Oxford, 2002).
[18]P. Willmott, *An Introduction to Synchrotron Radiation: Techniques and Applications* (Wiley, Chichester, 2011).
[19]S. Hirschi, J. L. Schwartz and R. L. Whiddon, "A film loop: Synchrotron radiation," Am. J. Phys. **41**, 836–838 (1973).
[20]Center for X-Ray Optics, Lawrence Berkeley National Laboratory, Berkeley, <www.cxro.lbl.gov/x-ray-data-booklet>.
[21]D. Attwood, *Soft X-Rays and Extreme Ultraviolet Radiation: Principles and Applications* (Cambridge U.P., Cambridge, 2007). Online lectures are accessible at <webcast.berkeley.edu/course_details.php?seriesid=1906978420>.
[22]J. Schwinger, "On the classical radiation of accelerated electrons," Phys. Rev. **75**, 1912–1925 (1949).
[23]V. O. Kostroun, "Simple numerical evaluation of modified Bessel functions of fractional order," Nucl. Instr. Methods **172**, 371–374 (1980).
[24]C. A. Brau, "Undulator radiation," Am. J. Phys. **64**, 662–666 (1996).